Anomalous structural response of nematic colloidal platelets subjected to large amplitude stress oscillations

O. Korculanin, D. Hermida-Merino, H. Hirsemann, B. Struth, S. A. Rogers, and M. P. Lettinga

Citation: Physics of Fluids **29**, 023102 (2017); doi: 10.1063/1.4975605
View online: http://dx.doi.org/10.1063/1.4975605
View Table of Contents: http://aip.scitation.org/toc/phf/29/2
Published by the American Institute of Physics

Anomalous structural response of nematic colloidal platelets subjected to large amplitude stress oscillations

O. Korculanin,[1,2] D. Hermida-Merino,[3] H. Hirsemann,[4] B. Struth,[4] S. A. Rogers,[5] and M. P. Lettinga[1,2,a)]

[1]*ICS-3, Forschungszentrum Jülich GmbH, 52428 Jülich, Germany*
[2]*Laboratory for Soft Matter and Biophysics, KU Leuven, B-3001 Leuven, Belgium*
[3]*DUBBLE CRG BM26@ESRF, 38043 Grenoble, France*
[4]*DESY, 22607 Hamburg, Germany*
[5]*Department of Chemical and Biomolecular Engineering, University of Illinois Urbana-Champaign, Champaign, Illinois 61801, USA*

(Received 2 September 2016; accepted 23 January 2017; published online 22 February 2017)

Time-resolved small angle X-ray measurements are used to investigate the dynamic response to nonlinear oscillatory stresses and strains of a nematic dispersion of colloidal gibbsite platelets. We track the full 3D rotational motion of the director by employing plate-plate and concentric cylinder Couette geometries as well as a vertical X-ray beam. Under nonlinear oscillatory stress, we observe strong offsets in the rheological response as well as asymmetrical behavior in the microscopic structural response. This offset and asymmetry are connected to the yielding behavior of the platelets. By increasing the stress amplitude, we observed that the offset of the rheological response diminishes and the microscopic response becomes more symmetric; however, this strongly depends on the frequency of the stress input, and hence the time necessary for the system to yield. [http://dx.doi.org/10.1063/1.4975605]

I. INTRODUCTION

Anisometric colloids have a wide range of applications across a variety of industries (food, cosmetics, and drilling fluids) due to their rich rheological properties. Naturally occurring clays are an important example of anisometric colloids as they are generally platelets that contain metal oxides and organic materials. At high concentrations, suspensions of these platelets often form isotropic physical gels rather than the orientationally ordered nematic phase that is expected for anisotropic systems. This is due to short-range interactions between the colloids that result from the inhomogeneous surface charge distribution.[1] Platelets that carry different charge on the face and edges display the so-called "house of cards" effect. Coussot *et al.*[2] showed that the "house of cards," in their case formed by suspensions of the artificial clay laponite, can exhibit "avalanches" in creep tests. The suspensions were observed to creep slowly at stresses above their ultimate yield values before rapidly transitioning to a high shear rate response: the avalanche.

Gibbsite platelets have a homogeneous positive surface charge, which makes the suspension charge-stabilized and, as such, they can achieve a nematic phase state at high concentrations. In their work, ten Brinke *et al.*[3] and Michot *et al.*[1] have shown that apart from surface charge distribution, factors such as platelet size, aspect ratio, and polydispersity play a role in the material properties of the system, including the yield stress of the dispersion. Nonetheless, these systems display the phase transitions to liquid crystalline states expected for platelets.[4] In a previous paper, we identified a dynamic yielding transition under large amplitude oscillatory (LAO) shear deformations of gibbsite suspensions in the nematic phase from elastic to plastic deformation, accompanied by a flipping of the nematic director.[5] By employing a semi-quantitative analysis method, similar to that proposed by Rogers,[6] in which the transient stress response is viewed as being the result of a sequence of physical processes (SPP), we were able to form a dynamic structure-property relationship.

Yielding mechanisms are, however, prone to be very different when stress is applied instead of strain, especially for an ordered system such as the nematic gibbsite dispersions. Thus, a complete characterization of a nonlinear material response cannot be gained by performing strain-controlled tests alone but must also be accompanied by nonlinear stressing, as argued for in Refs. 7–9. The majority of dynamic nonlinear rheological investigations of soft materials have focused on the periodic stress responses to large oscillating strains, while the periodic strain responses induced by large amplitude oscillatory stresses have been studied much more infrequently. A review by Hyun *et al.*[10] of the large-amplitude oscillatory shear literature was published in 2011, in which no stress-controlled data are presented or discussed. Further, the techniques presented in that review have been shown by Rogers and Lettinga[11] to be poorly suited to describing yielding responses due to their overly strict assumptions. Läuger and Stettin[12] investigated the nonlinear responses of various materials to both strain and stress excitations, providing quantitative analysis in support of this concept. Dimitriou, Ewoldt,

a)Author to whom correspondence should be addressed. Electronic mail: p.lettinga@fz-juelich.de

and McKinley[8] proposed a new nomenclature to differentiate the effects of each paradigm, suggesting the terms LAOStrain and LAOStress be used to describe Large Amplitude Oscillatory Strain/Stress. Periodic strain responses to oscillatory shear stresses have been investigated in Refs. 8 and 12–15. With the exception of the Dimitriou, Ewoldt, and McKinley[8] work, all of these have investigated the ability of stress-controlled rheometers, in which the motor and transducer are combined, to replicate the strain-controlled conditions of rheometers in which the motor and transducer are separated. Some issues that can affect the data obtained from a rheometer include torque and displacement limits, surface tension forces, and volume effects. Mechanisms for identifying and avoiding regions of "bad" rheometrical data have been discussed at length recently.[16] In addition to the relative dearth of oscillatory stress literature, it is not even clear within the existing literature how oscillatory stresses should be described. Earlier works employ the standard of describing oscillatory stresses as being sinusoidal, while recently Ewoldt[9] suggested that oscillatory stresses ought to be cosinusoidal for reasons to do with signs of Fourier coefficients and where one chooses to call the "start" of the oscillation. In this work we present the results of an investigation into the nonlinear response of hexagonal gibbsite platelets suspended in glycerol to LAOStress. For the analysis of the mechanical response, we employ the fully quantitative SPP approach, which is immune to the issue of when one chooses to call "the start" of a periodic response. Contrary to Fourier-based approaches, within the SPP framework, results are identical if one chooses to refer to the input as a sinusoid or cosinusoid.

In the study of viscoplastic materials, such as the nematic gibbsite dispersion, determination of the (apparent) yield conditions is paramount. Associated with such measurements is the importance of the time scale over which the measurements are made. The aforementioned seminal work on the "avalanche effect" during creep tests on the artificial clay (laponite) suspensions showed that the stress is not the only important parameter for determining yielding of the material. The time at which solidification, or a monotonic increase in the viscosity with time, occurs was observed to be a function of the inverse of the difference between the applied stress and the ultimate yielding criterion. Many researchers have referred to this phenomenon as a viscosity bifurcation.[2,17,18] Stresses less than, but very close to, the yield value could therefore appear to flow with a steady and stable low apparent viscosity for an extended interval of time before flow ceases and the viscosity steadily rises without an upper bound.

In their study of the rheology of colloidal gels, Sprakel *et al.*[19] investigated the phenomenon of delayed yield, in which yielding was only observed after stressing for times that were inversely proportional to the applied loading. This behavior is similar to the viscosity bifurcation observed by Coussot *et al.*,[2] in that the material responses are exquisitely sensitive to the combination of time and stress. However, in the case of delayed yielding of colloidal gels, the viscosity is observed to increase in time before rapidly decreasing at some later time, while in the viscosity bifurcation, the opposite trends in viscosity evolution are observed. Sprakel *et al.*[19] explained delayed yield in colloidal gels in terms of a bond rupture model that quantitatively described their results and highlighted the role of mesoscopic structures.

While it is clear that under constant stress conditions, as in traditional creep tests, some viscoplastic materials undergo a slow structural transition that eventually leads to avalanche-type or delayed yield behavior, the response of soft systems to dynamic stressing is less clear. Using LAOStress protocols, a natural time scale of the experiment is set by the applied frequency as opposed to a creep test. By controlling the magnitude of the stress and the time scale over which it is varied, it may be possible to place the material into a state that cannot exist under static conditions. The specific structural transitions the material exhibits within the period of oscillation will depend on both the stress amplitude and the duration of the oscillation. The nematic gibbsite dispersions are an ideal system to test these concepts given the clear yielding signature of the structural response using time-resolved small angle X-ray scattering (SAXS). In order to follow the orientation of the nematic structure over the full period of the oscillation, it is important that both the flow-gradient (1-2) and flow-vorticity (1-3) planes are probed. We therefore present here *in situ* LAOStress measurements using both Couette and plate-plate geometries in combination with the vertical beam setup.

The paper is organized as follows. In Section II we describe the experimental setup, the materials studied, and we elucidate the features of the two shear geometries that were employed in combination with the vertical beam X-ray setup. In Sec. III, we introduce typical mechanical and structural responses and describe how the relevant scalars we use to characterize these responses are extracted. Sec. IV is naturally divided into three parts, in which we present results from the alteration of distinct experimental parameters. First we discuss the stress amplitude dependence of the characterization scalars, focusing on the yielding of the fluid. We then demonstrate the effect of the frequency of oscillation on the yielding behavior. Finally, we finish with a discussion.

II. EXPERIMENTAL

A. Setup

We used a stress-controlled MARS III rheometer (Thermo Fischer, Germany) which is suitable for LAOStress, and at the applied frequencies it can be also operated in LAOStrain mode. A partially coherent X-ray beam was deflected by germanium crystal optics by 90°, resulting in a vertical X-ray beam, passing through the geometry, parallel to the rotation axis of the rheometer around 14 mm from the rheometer axis. This setup is a mobile version of the pilot installation by Struth *et al.*[20] and was installed at the Dutch-Belgian beamline BM26B (DUBBLE) of the European Synchrotron Radiation Facility (ESRF)[21,22] in Grenoble, France, using a beam that has a photon energy of 8.05 keV, corresponding to a wavelength of $\lambda = 0.15$ nm.

The advantage of our setup is that one can easily exchange shear geometries and therefore probe different scattering planes. In this work we employ plate-plate and concentric-cylinder Couette geometries. In the plate-plate geometry the beam is directed along the gradient-of-velocity direction $\nabla \mathbf{v}$ (in short gradient or 2 direction), probing structures that scatter

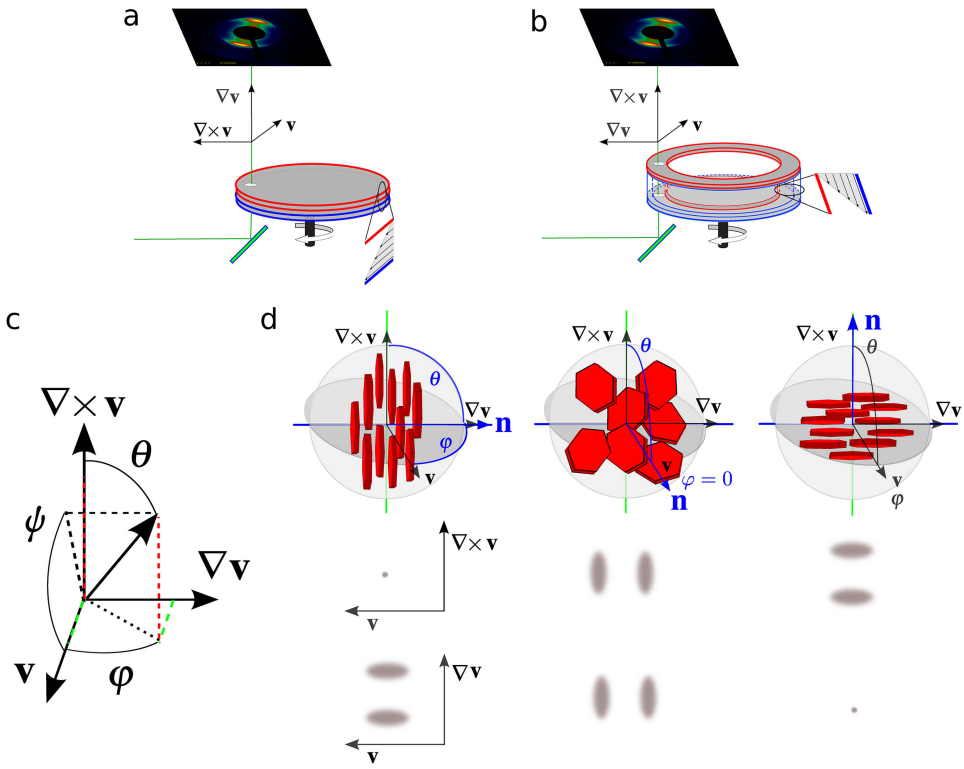

FIG. 1. Sketch of the two scattering geometries used, (a) plate-plate and (b) Couette geometry, where the X-ray beam (indicated by green line) is reflected vertically by a germanium crystal. (c) Depicts the angles of the nematic director in the scattering space and (d) the different orientations of the nematic phase and their predicted scatter pattern, depending on the scatter geometry.

in the flow-vorticity plane (also $\mathbf{v} - \boldsymbol{\nabla} \times \mathbf{v}$ plane or 1 – 3 plane). In the Couette geometry the beam is directed along the vorticity direction so that the flow-gradient scattering ($\mathbf{v} - \boldsymbol{\nabla}\mathbf{v}$ or 1 – 2) plane is probed. Fig. 1 shows both geometries and indicates the angles that define the orientation of anisotropic structures, and therefore the nematic director in terms of the azimuthal angle φ and polar angle θ. Thus, with the Couette geometry we obtain the azimuthal angle φ, while with the plate-plate geometry, we obtain the angle ψ, which is the projection of the scattering on the $\mathbf{v} - \boldsymbol{\nabla} \times \mathbf{v}$ plane.

The Couette geometry consists of two concentric cylinders with diameters of 30 and 28 mm, so that the gap is 1.0 mm, while the height of the cylinders is 3.0 mm. The measurements in Couette geometry were performed in the middle of the sample cell's gap. A gap of 1.0 mm was used in the plate-plate geometry. Both geometries are home-made and fabricated from polyimide (Vespel, DuPont) to reduce X-ray absorption at moderate X-ray energies. Throughout the experiments we observed that the mechanical responses of the system are qualitatively very similar for the geometry used. However, as we will report later, the absolute stress differ significantly, this is mainly due to the inhomogeneous stress in the plate-plate geometry. Hence, we only report apparent stress in the paper, due to the radial inhomogeneity especially for the plate-plate geometry.

For the detection of anisotropic scattering patterns, the novel LAMBDA detector,[23,24] a 2D photon counting detector, developed at DESY, Hamburg was used. The LAMBDA has a high spatial resolution with a pixel size of $55 \times 55\ \mu m^2$, a high quantum efficiency close to 100%, and a high speed acquisition of up to 2000 frames/s. Thus, the temporal resolution of the experiment was determined by the flux of the beam, resulting in a minimum of 0.25 s/frame. The LAMBDA

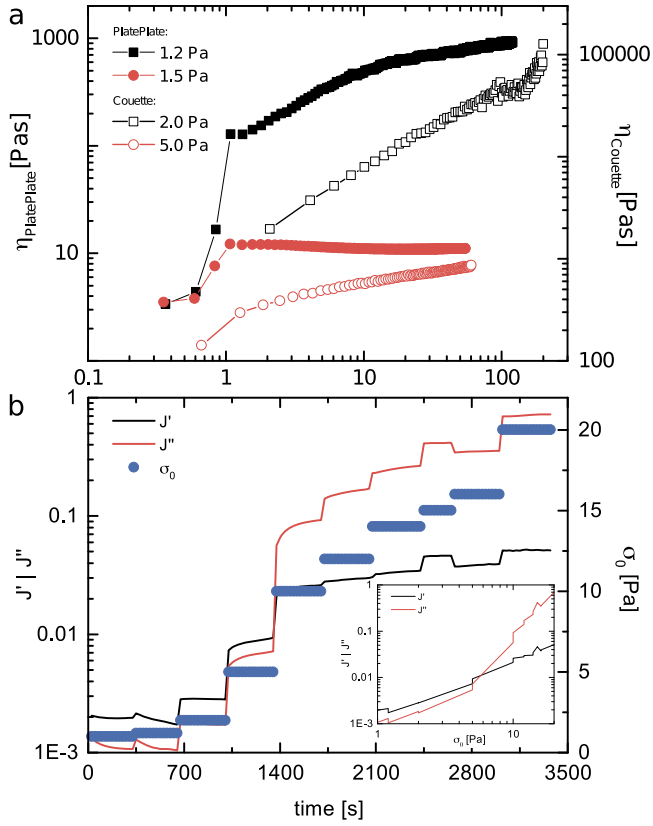

FIG. 2. Creep results for the suspension in terms of (a) the viscosity for the plate-plate (closed) and Couette (open symbols) geometry. The range of stresses at which the system yields into a flowing material, lie between 1.2 and 1.5 Pa for the plate-plate, and between 2.0 and 5.0 Pa for the Couette geometry. Dynamic stress sweep performed in Couette geometry over time (b) and over applied stress amplitude ((b), inset), calculated by Eq. (3), at 0.04 Hz, shows yielding between 5 and 10 Pa.

was placed at a distance $R_{det} \approx 2.1$ m downstream of the sample position, yielding a q-range $q_{max} \approx 0.1135\,\text{nm}^{-1}$, which corresponds to a face-to-face platelet distance of 55 nm, similar to the nematic-ordered gel in Ref. 25. The distance between rheometer and detector was bridged by a flight tube filled with helium to minimize air scattering.

B. Materials

The colloidal platelets studied are made in-house, following a procedure from Ref. 26. They are gibbsite ($\gamma - Al(OH)_3$) hexagonal shaped particles with a positively charged surface, a thickness $L = 8.4 \pm 2.8$ nm, and a diameter of $D = 250 \pm 32$ nm. The gibbsite platelets were dispersed in water saturated glycerol at a volume fraction of 12.7% where the suspension is in the nematic phase.

The bounds of the yield stress of this material, which serve as a reference for the stress-controlled LAOS measurements, were measured in both geometries, as presented in Fig. 2(a). In the Couette geometry, the static yield stress is between 2.0 and 5.0 Pa, while for the plate-plate geometry it is between 1.2 and 1.5 Pa. As mentioned above, the discrepancy is purely experimental and a precise determination is not the focus of this work. Instead, we seek to investigate the structural responses to oscillatory inputs that are much less than, much more than, and approximately equal to these values. Indeed, Fig. 2(b) shows a yielding where $J' < J''$ between stress amplitudes of 5 and 10 Pa. The data are obtained during the measurements that we present in Section IV. Furthermore, the amplitude of the applied oscillations was chosen such that the mechanical responses were of comparable magnitude for both planes.

III. ANALYSIS

A. Parameterizing the structural response

Typical scattering patterns of sheared nematic gibbsite dispersions are shown in Figs. 3(c)–3(f) for both scattering geometries used, where a clear nematic structure peak can be observed both in the $\mathbf{v} - \boldsymbol{\nabla} \times \mathbf{v}$ and $\mathbf{v} - \boldsymbol{\nabla}\mathbf{v}$ planes. In the first step of the analysis, we link these patterns to the orientational distribution of the platelets given by $f(\varphi, \theta)$. The average orientation of the platelets, and thus the director, is given by the angles φ_{max} and θ_{max} where $f(\varphi, \theta)$ has its maximum. The width of the orientational distribution around this director gives a measure of the orientational ordering of the system.

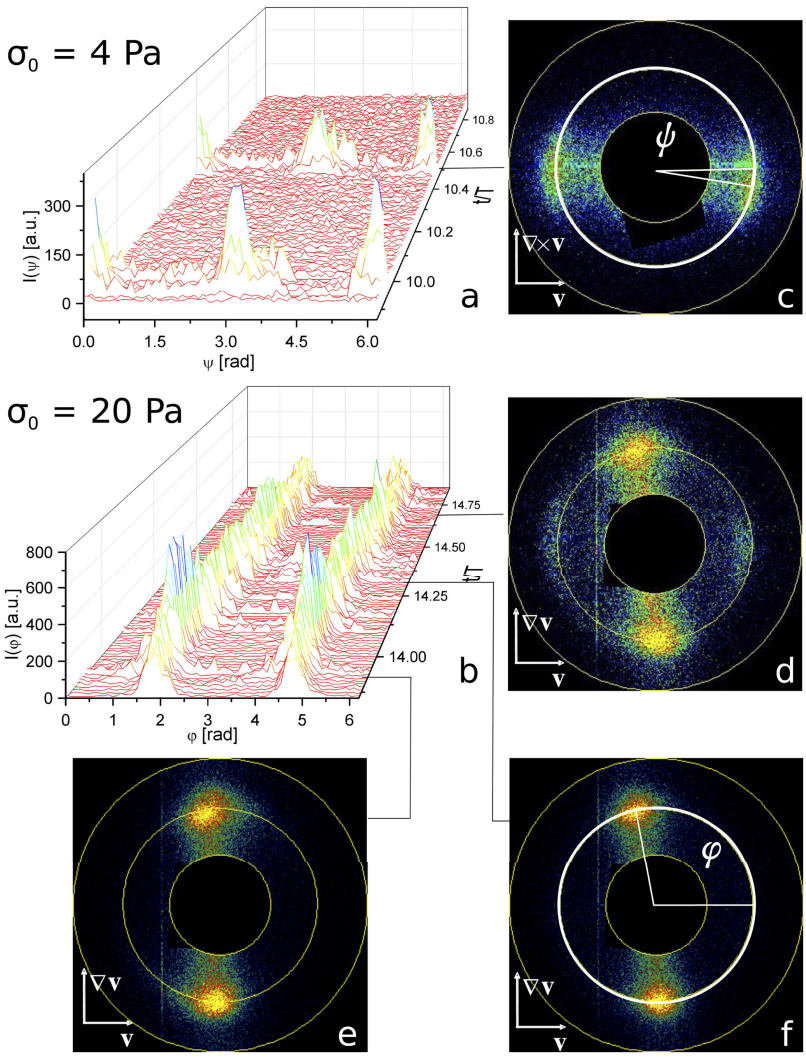

FIG. 3. 3D representation of the measured scattering intensity over the angles (a) ψ and (b) φ along the period, in the plate-plate and Couette geometry, respectively. Data acquired at mid range frequency, 0.04 Hz, and at stress amplitudes well above the yield stress for both scattering planes. The X-ray images ((c)-(f)) are snap-shots taken at the indicated times, with the subsequent angles and scattering planes marked in the images.

In the scattering experiments we cannot directly measure $f(\varphi, \theta)$, but instead we measure its projections onto the two available scattering planes. To quantify the ordering, the scattering patterns are first reduced to intensity profiles, plotting the integrated intensity at q_{max} versus ψ and φ, respectively, as indicated by the white circles in Figs. 3(c) and 3(f). Next, we assume that $f(\psi)$ and $f(\varphi)$ are proportional to the respective intensity profiles, as in Ref. 28. Such profiles are displayed in Figs. 3(a) and 3(b) during a stress oscillation. A noteworthy observation is that there is an extra limitation in obtaining these functions, as the nematic structure peak is only observed when the director has a sufficient tilt away from the incident beam, as illustrated in Fig. 1. To observe the structure peak in the $\mathbf{v}-\nabla\mathbf{v}$ plane, the requirement is that $\theta_{max} \in 90 \pm \Delta\theta$. To observe the structure peak in the $\mathbf{v} - \nabla \times \mathbf{v}$ plane, the requirement is that $\varphi_{max} \in 0 \pm \Delta\varphi$.

The last step in the analysis is to parameterize the orientational ordering by single scalars. To this end, we fit these functions with a Maier-Saupe type of orientation distribution function,

$$I(\psi|_{q_{max}}) = I_0 \exp[\alpha P_2(\psi - \psi_{max}) - 1], \tag{1}$$

where I_0 is the amplitude, α describes the width of the intensity profile, and $P_2(\psi) = \frac{1}{2}(3\cos(\psi - \psi_{max})^2 - 1)$ is the second Legendre polynomial, allowing for the director to point along ψ_{max}. A better quantification of the ordering is to calculate the average orientational order parameter $\langle P_2(\psi)\rangle$, which can be calculated using the fitted parameters,

$$\langle P_2(\psi)\rangle = \frac{\int_0^{\pi} \exp[\alpha P_2(\psi - \psi_{max})] P_2(\psi - \psi_{max}) \sin(\psi) d\psi}{\int_0^{\pi} \exp[\alpha P_2(\psi - \psi_{max})] \sin(\psi) d\psi}. \tag{2}$$

In this way the scattering response is reduced to a function of the three parameters $\langle P_2(\psi)\rangle$, ψ_{max}, and I_0. The latter parameter is useful as it indicates whether the condition $[\theta_{max} \in 90 \pm \Delta\theta]$ is fulfilled, and therefore it is an indication for θ_{max}, which in principle is not probed in this plane. Identical parameters can be obtained for $f(\varphi)$ in a similar manner. When discussing the effect of stress amplitude and frequency on the structural response we will always refer to these parameters.

B. Mechanical characterization

When performing oscillatory rheological measurements, a choice must be made as to how the results are viewed and analyzed. Early investigations (see Refs. 29–33), which were performed within the LAOStrain paradigm, viewed the responses as periodic time series, and so naturally Fourier transformed the data. A number of departures from this approach have been presented and discussed in recent literature (see Refs. 6, 11, 34, and 35). Here, we employ a technique where the response of the material is viewed as being a sequence of processes (SPP) that are dependent on the applied fields, which in this case are the stress and stress-rate. This framework has been shown[6] to be ideally suited to investigations of yielding responses and is immune to the issues raised by Ewoldt[9] regarding where in an oscillation one chooses to refer to as the "start." Given this immunity, there is no need to change our description of the stress to another trigonometric function, and we retain the sinusoidal description that is nearly universally employed in the literature. In addition to the clarity of the physical interpretations and the unparalleled time resolution afforded by this approach, we see the immunity to where one calls the "start" as a major strength of this technique. In the linear rheological regime, we describe the strain response $\gamma(t)$ to an oscillatory stress of amplitude σ_0 and angular frequency ω of the form $\sigma(t) = \sigma_0 \sin(\omega t)$ in terms of the real and imaginary components of the complex compliance, J' and J'' as

$$\begin{aligned}\gamma(t) &= \sigma_0 [J' \sin(\omega t) - J'' \cos(\omega t)] \\ &= J'\sigma(t) - \frac{J''\dot{\sigma}(t)}{\omega}.\end{aligned} \tag{3}$$

The second form of Eq. (3) can be rearranged with little effort into the general form of the equation of a plane in $[\sigma(t), -\dot{\sigma}(t), \gamma(t)]$ space with a normal vector pointing in the direction of $[J', J'', -1]$, with zero offset in the $\gamma(t)$ direction,

$$J'\sigma(t) - \frac{J''\dot{\sigma}(t)}{\omega} - \gamma(t) + 0 = 0. \tag{4}$$

One can use the formalism of the Frenet-Serret apparatus and say that such a trajectory has a time-independent binormal vector,[6] $\mathbf{B} = [B_\sigma, B_{-\dot{\sigma}}, B_\gamma]$, pointing in the direction of $[J', J'', -1]$. Extension to arbitrary nonlinear responses within this sequence of physical processes framework is achieved by mapping the orientation and position of the osculating plane, and therefore the binormal vector, during an oscillation. By taking the position of the osculating plane into account, a simple definition of transient viscoelastic parameters is obtained. This process, which is outlined briefly here, and detailed in Rogers (submitted) yields time-dependent compliances defined by the measured components of the binormal vector,

$$J'(t) = \frac{B_\sigma}{B_\gamma}, \tag{5}$$

$$J''(t) = \frac{B_{-\dot{\sigma}}}{B_\gamma}. \tag{6}$$

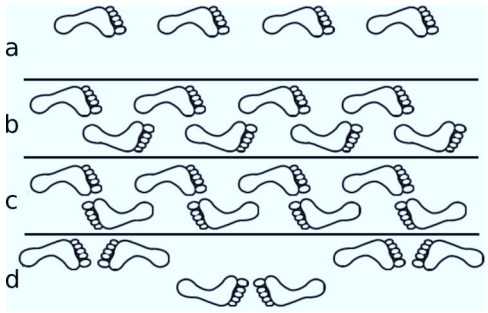

FIG. 4. Four of the seven frieze groups, which are 2D time symmetries, illustrated by a single left foot as a unit cell: (a) hop, with only translational symmetry; (b) step, with translational and glide reflection symmetry; (c) spinning hop, with translational and 180° rotation symmetry; and (d) spinning sidle, with translation, glide reflection, and 180° rotation symmetry. Adapted from S. A. Rogers and D. Vlassopoulos, J. Rheol. **54**, 859 (2010). Copyright 2010 by The Society of Rheology, Inc.[27]

The definitions of Equations (5) and (6) are generic in terms of the way they define the transient viscoelastic parameters. The difference between the definitions presented here for stress-controlled parameters and those presented elsewhere (Rogers[6] and submitted) for strain-controlled methodologies is the space in which the trajectories are said to lie. The binormal vectors are therefore defined in terms of different parameters, meaning that linear viscoelastic responses will transform between stress- and strain-controlled methodologies in the usual manner, while significant differences in the parameters are observed in the nonlinear regime. This technique is unique in that it allows researchers to follow the relative contributions to the strain response from the in- and out-of-phase components of the complex compliance during an oscillation. Further, a subtle distinction is made between strains in the lab and material frames. The lab-frame strain is simply the measure reported by the rheometer, while the material-frame strain is the deformation to which the material responds. For instance, if an elastoviscoplastic material is made to flow, it will lose any memory of the lab-frame strain equilibrium. When flow is ceased, the material-frame strain will be zero, while the lab-frame strain will be dependent on the flow rate and duration. See, for instance, the investigations in Refs. 11 and 36–39 into the responses of yielding materials and models under LAOStrain.

Rogers and Vlassopoulos[27] suggested an enhancement to the rheology terminology, by introducing orbifold notation popularized by Conway[40,41] to better describe the response of a system in the time domain under oscillatory strain or stress. Discrete repeating patterns of an oscillating field propagating in time are represented by seven possible groups of symmetries, i.e., frieze groups, see Fig. 4. The new vocabulary

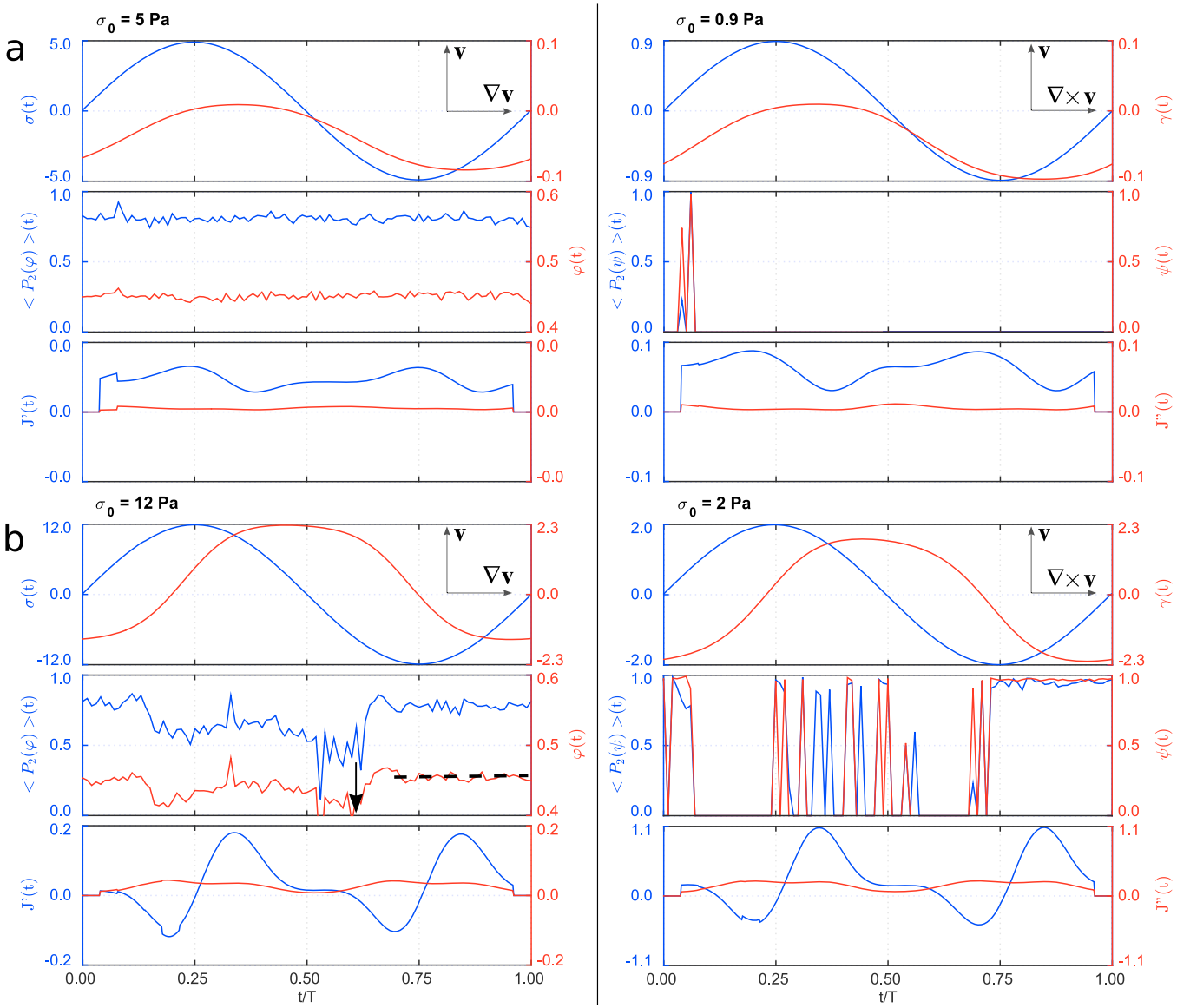

FIG. 5. Responses for two applied stress amplitudes both at 0.04 Hz in the $\mathbf{v} - \boldsymbol{\nabla}\mathbf{v}$ plane (left) compared to the apparent stress amplitude yielding a similar strain amplitude in the $\mathbf{v} - \boldsymbol{\nabla} \times \mathbf{v}$ plane (right). Stress amplitudes (a) well bellow yielding and (b) start of transition phase. The sub-graphs present: top, applied stress oscillation σ (blue) and strain response γ (red); middle, orientational order parameter $\langle P_2(\varphi)\rangle$ and $\langle P_2(\psi)\rangle$ (blue) and orientation of the nematic director φ and ψ (red), the arrow (black) points to the peak and dashed line (black) to the plateau value of $\varphi(t)$; bottom, time-resolved storage compliance $J'(t)$ (blue) and loss compliance $J''(t)$ (red) over the last period.

is suitable to describe any system, offering precise definitions of symmetric or asymmetric response to LAOStress or LAOStrain. Generally, it is assumed that a linear response is represented by a spinning sidle frieze, where the path to local extrema is retraced on the return toward equilibrium, see Fig. 4(d) and a step frieze, in which the paths to and from local extrema need not be the same; Fig. 4(b) is a nonlinear rheological response.

IV. RESULTS

A. Stress amplitude dependence

In this section we decouple the effects of the applied stress amplitude and the frequency on the strain response. The first step of this process involves identifying what stress amplitude σ_0 is required to make the system flow at least for part of the oscillation, making use of the nonlinear compliances defined in Eqs. (5) and (6). The time response of all relevant rheological and structural parameters for amplitudes below and just around the yield stress, identified previously, is given in Fig. 5, while the responses for amplitudes larger than the yield stress are given in Fig. 6.

The mechanical responses at *stress amplitudes below the yield stress*, given in the top panels of Fig. 5 for both geometries (σ_0 = 5 Pa and 0.9 Pa), indicate a solid-like response, as $J'(t) >> J''(t)$. Note, however, that the response of the strain oscillates about a non-zero value of around −0.05. This strain is irreversibly acquired during the transient approach to steady state. We believe strain offsets to be physically meaningful, and an integral part of stress-controlled oscillatory rheometry. We report the raw data here for completeness, with a scaling by the amplitude as the only data treatment, for future reference. The SPP framework employed here is able to handle the offset and there is no need to post-treat the data. We will not focus in this work on their physical cause and reserve their study for an upcoming publication. The structure response, as determined by the scattering parameters, does not show any

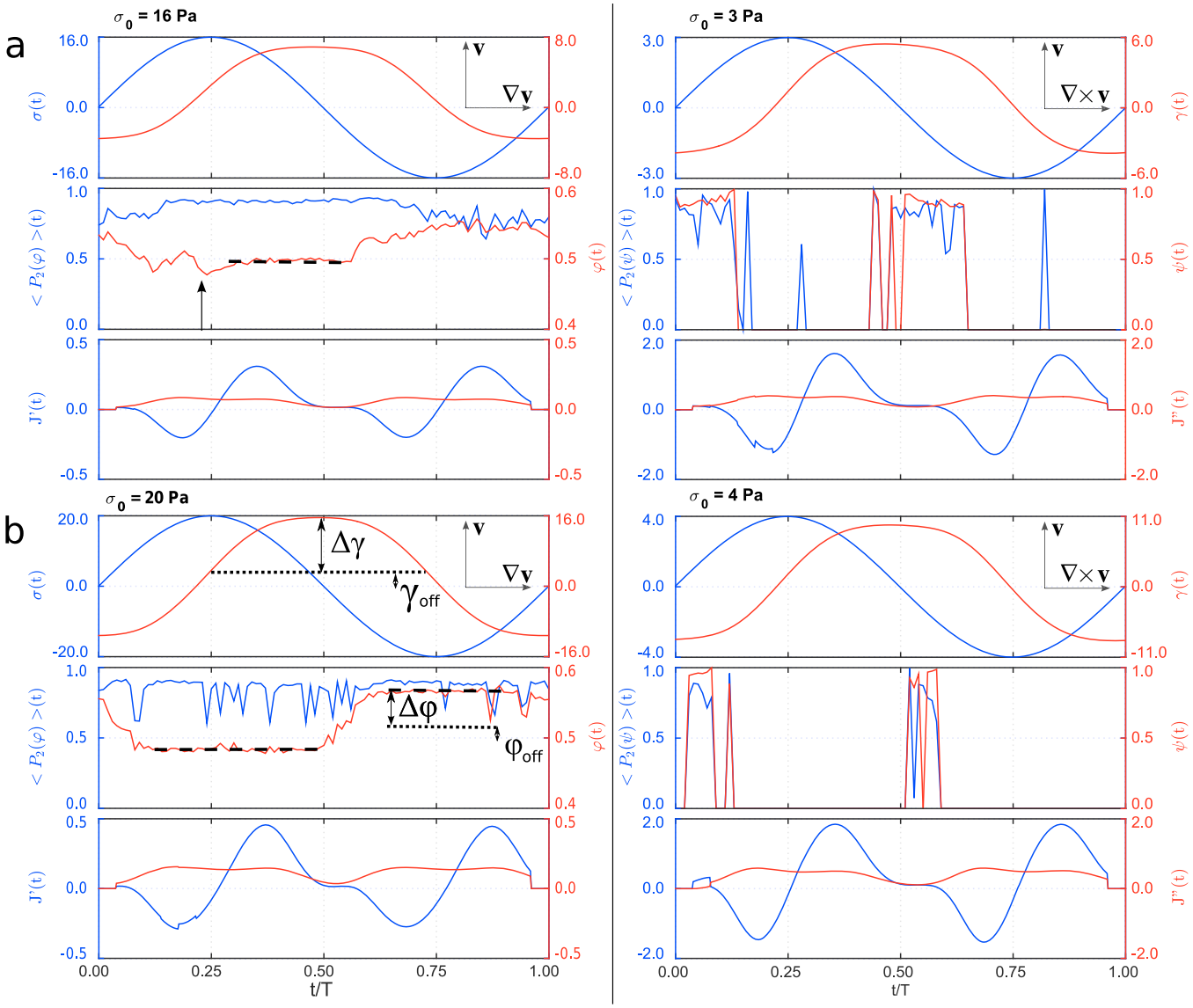

FIG. 6. Responses for two applied stress amplitudes at 0.04 Hz in the $\mathbf{v} - \nabla\mathbf{v}$ plane (left) compared to the apparent stress amplitude yielding a similar strain amplitude in the $\mathbf{v} - \nabla \times \mathbf{v}$ plane (right). Stress amplitudes at (a) transition, with arrow pointing to the peak and dashed line to the plateau value of $\varphi(t)$; (b) well above yielding, with arrows depicting the amplitude and the dotted line is the vertical offset in the response.

features throughout the full oscillation. The orientational order parameter, $\langle P_2(\varphi)\rangle$, is constantly high, indicating a high ordering of φ with the director oriented at a small angle with the normal of the wall. According to Conway's orbifold notation, both $\langle P_2(\varphi)\rangle(t)$ and $\varphi(t)$ are hop friezes, where a spinning sidle in $\gamma(t)$ leads to hop frieze in $J'(t)$. It is worth mentioning here that the angle $\varphi(t)$ depends on the history of the system: as steady shear was applied before the start of the oscillatory measurement, this shear-induced angle did not relax over the time of the experiment. Combining the structural and mechanical responses, it can be seen that at stress amplitudes less than the yield stress, the system is frozen in whatever state it was left in due to any pre-shear protocol.

The mechanical response at *stress amplitudes well above the yield stress*, given in Fig. 6(b) (σ_0 = 20 Pa and 4 Pa), shows a clear yielding region around stress reversal, where $J'(t) < J''(t)$ for a considerable part of the period before $J'(t)$ goes negative and the system recoils during a short time interval. Moreover, $\gamma(t)$ appears to oscillate about a value closer to zero as compared to the smaller stress amplitudes. Enforcing yielding at such large stress amplitudes therefore acts to negate the transience observed at stress amplitude less than the yield stress.

A prominent structural response underlies this mechanical yielding event. At the stress reversal, when $t/T = 0.5$, the director starts to tilt away from $\varphi = \frac{1}{2}\pi$. At the same time a sharply defined event in ψ and $\langle P_2(\psi)\rangle$ can also be detected in the $\mathbf{v} - \nabla \times \mathbf{v}$ plane, as the director quickly passes through the flow direction. This is very similar to the yielding response observed when applying large amplitude strain oscillations, where the events take place at the flow reversal.[5] The scheme of Fig. 1 suggests that reflections detected in the flow direction in the $\mathbf{v} - \nabla \times \mathbf{v}$ plane should be accompanied by similar reflections in the $\mathbf{v} - \nabla\mathbf{v}$ plane. Indeed, the tilting in φ is accompanied by the appearance of a second structure peak around $\varphi = 0$, which counter-rotates. This second peak is not as pronounced as the first, as can be seen in Fig. 3(d), but is more apparent in the supplementary material. Eventually, the side peak merges with the main peak at a tilted angle $\varphi \approx 0.57\pi$ when the stress reaches its minimum.

Looking at each of the phenomena as describing the same sequence of processes, we conclude that nematic domains split up as the director tilts away from the gradient direction at $t/T = 0.5$. Parts of the sample rotate towards the flow direction as well as the vorticity direction as the intensity decreases. However, the symmetry of the responses is markedly different: $\varphi(t)$ is a step frieze, while $\langle P_2(\varphi)\rangle(t)$ is a hop frieze and $J'(t)$ and $\gamma(t)$ are spinning hop friezes. In fact, spinning hop symmetry is a subgroup of the hop frieze group, consequently depending on the softness of the response. A possible explanation of this behavior is that the system does not fully yield throughout the complete oscillation as can be appreciated from the structural data: φ does not tilt towards values smaller than $\varphi \approx 0.48\pi$, while $\langle P_2(\varphi)\rangle$ fluctuates during the half of the period where φ is close to $\varphi = \frac{1}{2}\pi$ and the instantaneous stress decreases. Hence the system displays a bifurcation where the structure either is anchored by the wall with the director at $\varphi \approx 0.48\pi$ or in a flowing state with the director at an angle of $\varphi = 0.57\pi$, typical for flowing nematic (Leslie angle).

The *transition* between both responses is subtle. The strain response for σ_0 = 12 Pa (or 2 Pa in $\mathbf{v} - \nabla \times \mathbf{v}$ plane) exhibits yielding as $J'(t)$ crosses $J''(t)$, see Fig. 5(b), and is a spinning hop frieze, as observed for σ_0 = 20 Pa. Moreover, the offset in γ is less noticeable. The structural response is more complex as it shows regions where both $\langle P_2(\varphi)\rangle(t)$ and $\varphi(t)$ are independent of stress and time, indicated by the dashed lines in Figs. 5 and 6, as well as peaks in these parameters, indicated by the arrows. In the $\mathbf{v} - \nabla \times \mathbf{v}$ plane, observed in the plate-plate geometry, we see that there is a single frequency response and therefore a bifurcation in the response, though strong fluctuations are observed at the point where the flipping is expected. These fluctuations in both $\langle P_2(\varphi)\rangle$ and $\langle P_2(\psi)\rangle$, right before transition, as in Fig. 5(b), indicate jittering of the nematic director as the structure of the system breaks up during the yielding process. This structural response can be described as a hop symmetry with half the frequency. At σ_0 = 16 Pa (or 3 Pa in $\mathbf{v} - \nabla \times \mathbf{v}$ plane) the responses in $\langle P_2(\varphi)\rangle(t)$ and $\varphi(t)$ sharpen and the bifurcation for $\psi(t)$ disappears, see Fig. 6(a). However, with the disappearance of this bifurcation, i.e., we observe two reorientations per period, another bifurcation evolves: $\langle P_2(\varphi)\rangle(t)$ now responds to the sign of the stress rate. This response is therefore a hop frieze, as is the response in φ, contrary to the higher symmetric response for σ_0 = 20 Pa. The flipping event is also not as sharp as it is for σ_0 = 20 Pa. Moreover, there is a drop in the intensity and in $\langle P_2(\varphi)\rangle(t)$, at the moment that nematic structure breaks up. This suggests an incomplete reorientational motion of the director.

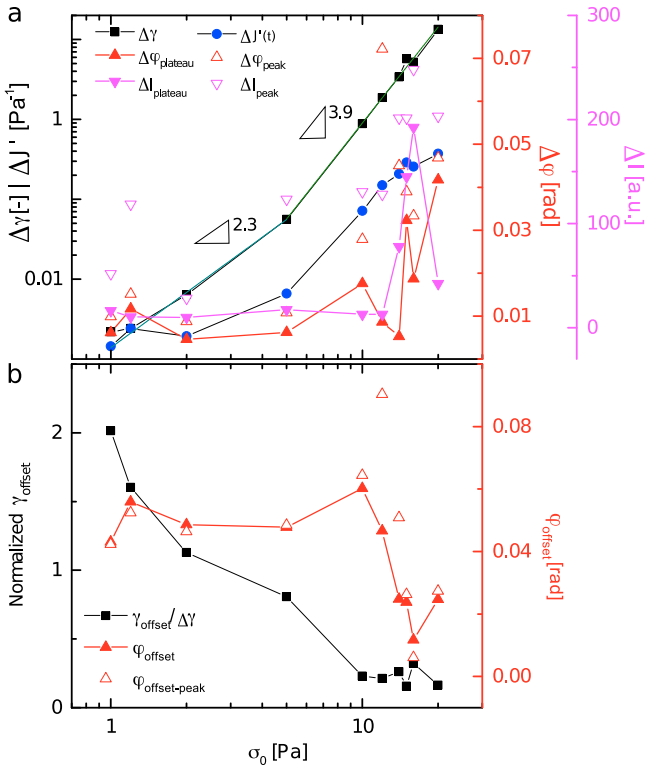

FIG. 7. Mechanical and structural response of the system depending on applied stress amplitude at fixed frequency 0.04 Hz: (a) the amplitudes of the responses and (b) the offset of the responses, where the offset in the mechanical response is normalized by its amplitude.

To quantify these observations and to pin down the dynamic yield stress, we further reduce the responses in terms of the amplitude and the offset in the responses of the parameters during a stress cycle. These values are summarized in Fig. 7 as a function of stress amplitude σ_0. The strongest response over the full range of σ_0 is clearly due to the strain amplitude $\Delta\gamma$ of the system, as can be appreciated from Fig. 7(a). The dependence of $\Delta\gamma$ on σ_0 is especially steep for stress amplitudes $\sigma_0 \gtrapprox 8$ Pa. The trend in the elasticity amplitude $\Delta J'$ is similar but less steep. For the structural response a distinction needs to be made between peak values (open symbols) and plateaus values (solid symbols), as indicated in Figs. 5 and 6. The amplitude of the scattering intensity, $\Delta I_{plateau}$ and $\Delta\varphi_{plateau}$, stays relatively flat up to a stress amplitude of $\sigma_0 \gtrapprox 10$ Pa, after which both parameters increase. This increase is more pronounced and seems to take place at lower σ_0 when considering the peak values. These observations, in accordance with the bulk rheological measurements presented earlier, suggest that above $\sigma_0 \gtrapprox 10$ Pa the system yields: $\Delta\gamma$ will just increase as it should for a fluid, while the director will settle at the Leslie angle known for liquid crystals.[42] A similar trend is observed when plotting the offset of the responses, as displayed in Fig. 7(b). Again, the strain response γ_{offset} continuously decreases with increasing σ_0, while a strong decrease in the structural response φ_{offset} is observed only when γ_{offset} settles at $\sigma_0 = 10$ Pa.

B. Frequency dependence

In Sec. IV A we discussed how events in a yielding process are correlated in time. As a finite amount of time is required for the system to yield, we discuss in this section the effect of the frequency on the LAOStress response. In Figs. 8(a) and 8(b), we compare the responses at the highest and lowest frequencies probed, respectively. Here σ_0 was kept fixed at 20 Pa for the Couette geometry, while we picked a stress amplitude for the plate-plate geometry that resulted in a similar strain response, as far as available.

We note a few remarkable differences. There is no structural yielding at high frequencies, despite the fact that

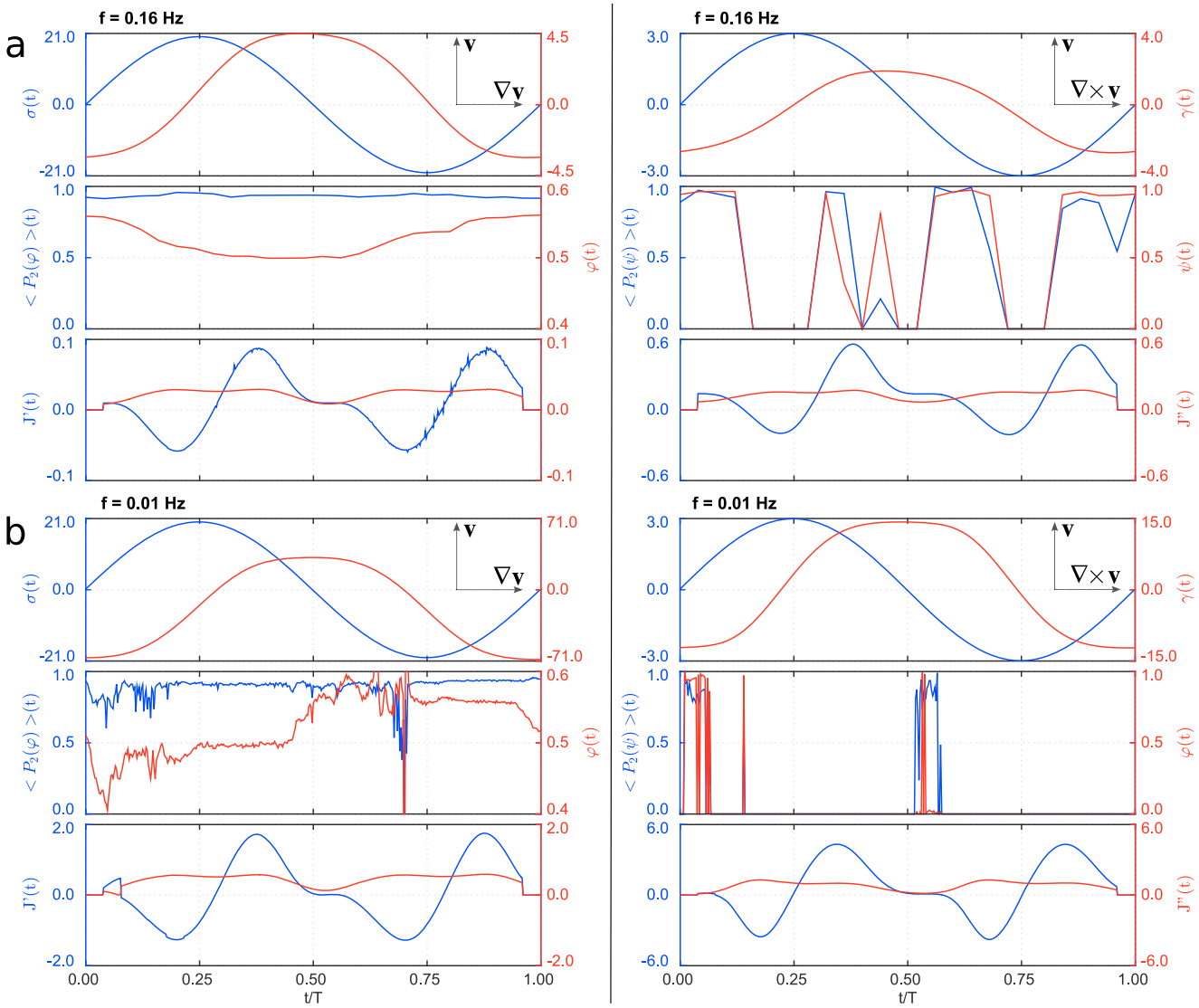

FIG. 8. The response at (a) highest and (b) lowest frequencies at stress amplitudes well above yielding in the $\mathbf{v} - \boldsymbol{\nabla}\mathbf{v}$ plane (left, 20 Pa) compared to the response at same frequency and similar strain amplitude in the $\mathbf{v} - \boldsymbol{\nabla} \times \mathbf{v}$ plane (right, 4 Pa).

$\sigma_0 \approx 2 \cdot \sigma_y$: the tilting angle φ shows a smooth quasi-linear profile, and the corresponding order parameter $\langle P_2(\varphi)\rangle(t)$ is high throughout the full period. This indicates that the director remains in the $\mathbf{v} - \boldsymbol{\nabla}\mathbf{v}$ plane, which is confirmed by the measurements in the $\mathbf{v} - \boldsymbol{\nabla} \times \mathbf{v}$ plane, where we only observe faint reflections. Thus, the time is too limited to perform a full reorientational motion of the director.

The middle frequency response, at 0.04 Hz that we have already seen in Fig. 6(b), where the profiles of $J'(t)$, $J''(t)$, and especially $\varphi(t)$ are more pronounced as compared to the high frequency response, indicates that the response is more nonlinear. At the lowest frequency we observe that $J'(t) \approx 0$, compared to $J''(t)$, meaning that for a short interval around the moment when the stress reverses at $t/T = 0.5$, elasticity is absent. This is the start of an interval when the structural response is erratic and where the intensity is also strongly reduced, indicating that many tumbling events take place into the vorticity direction, probably due to the reduced elasticity. $\Delta\varphi_{peak}$ also reaches extreme values at both sides of $\varphi = \frac{1}{2}\pi$. These events do not contribute to the stress response as the rheological response is still smooth. Note that the time-window in which the structural metrics are erratic corresponds to the point in the cycle where the system moves away from equilibrium where $\sigma_t = 0$. Thus, when the stress increases in magnitude, the structure response opposes the motion by jiggling around in both planes. Contrary to this behavior, the structure is immediately stable and $J'(t)$ is high when the stress is decreasing in magnitude, such that the wall alignment bifurcation for the bigger part is still intact. The width of the plateau region where $J'(t)$ is constant seems to decrease so that $J'(t)$ approaches a step frieze.

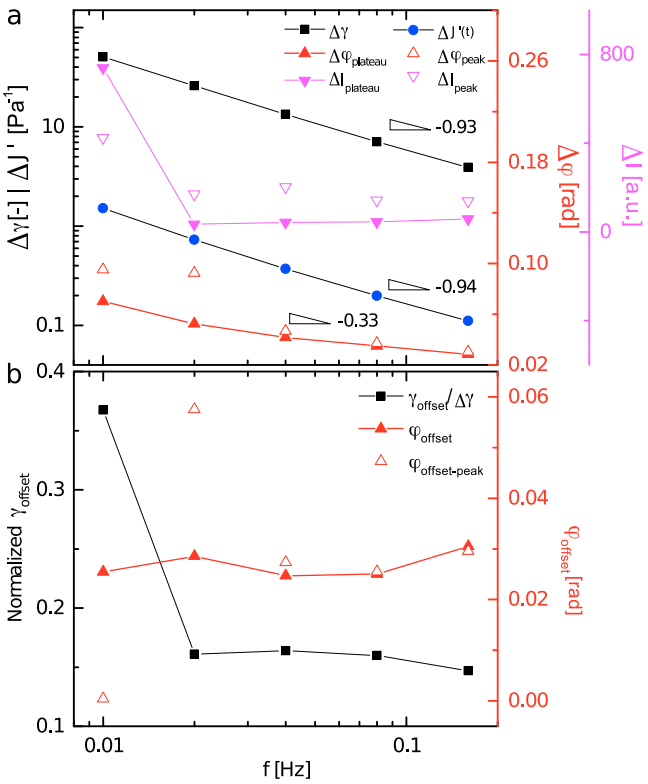

FIG. 9. Mechanical and structural responses of the system depending on frequency, range from 0.01 to 0.16 Hz, at 20 Pa applied oscillatory stress.

We quantify these observations again by plotting the amplitude and the offset in the responses of the parameters during a stress cycle, but now as a function of frequency, see Fig. 9. The strain and azimuthal angle amplitude linearly decrease with increasing frequency, with a slope of −0.93 and −0.33, respectively. The slope of −0.93 can be easily understood: as time of the period per oscillation decreases, the system has less time to develop a response to the applied force. Generally, the amplitudes of the rheological response, i.e., $\Delta\gamma$ and $\Delta J'$, are inversely proportional to the frequency, as the system has much more time to be deformed. The structural response is rather flat up to the lowest frequency. This complies with earlier strain controlled experiments where we found almost no frequency dependence. Only for the lowest frequency we observe dramatic changes. The mechanical response becomes very asymmetric, while the peaks in the structural response, given by the open symbols, become symmetric. In order to fully characterize this yielding, we would make measurements at even lower frequencies, an option that was not available in the experiment time.

C. Comparison between LAOStress and LAOStrain

There are a few important differences that can be observed between the response in strain or deformation and stress controlled LAOS. The large stress amplitude behavior, see Fig. 6, seems to be similar to the strain controlled experiment, with the breaking up and flipping of the director, see Fig. 10. The important difference is, however, that the LAOStrain response is more nonlinear, compared to the LAOStress response. This is apparent when comparing the width of the peak in $J'(t)$ and $G'(t)$, respectively. Moreover, the stress response is a spinning-hop frieze in time rather than a step frieze due to the more pronounced shoulder in the upturn of the stress response. The consequence is that the response of the structure, exemplified by $\varphi(t)$, does not show the bifurcation due to wall-anchoring as it is symmetric around $\varphi = \frac{1}{2}\pi$.

For small amplitudes we know that under strain control, the director will be always tilted such that reflections in the $\mathbf{v} - \boldsymbol{\nabla} \times \mathbf{v}$ plane will pop up, see Ref. 5. Contrary to this, for stress controlled experiments the structural response is constant in time, i.e., independent of the instantaneous deformation conditions, as can be seen in Fig. 5(a).

In other words, the system will always yield for strain controlled measurements, as the system is forced to flow. The enforced flow goes at the cost of more nonlinear behavior. This is especially the case for the mechanical response: the width of the peaks in $J'(t)$ is much smaller for the strain controlled measurements while $J''(t)$ is even close to independent of the applied stress. From the SAXS measurements we learn that the system can respond by choosing the path of least resistance to reorient the nematic director, depending on the amplitude of the applied force, in contrast to the enforced flip as observed in LAOStrain measurements.

Another very important difference is that we did not observe any frequency dependence for LAOStrain, while for LAOStress, at long time scales the system becomes nonlinear. The two methodologies do have in common that the yielding for both LAOStrain and LAOStress occurs at the moment where the sign of the applied field changes.

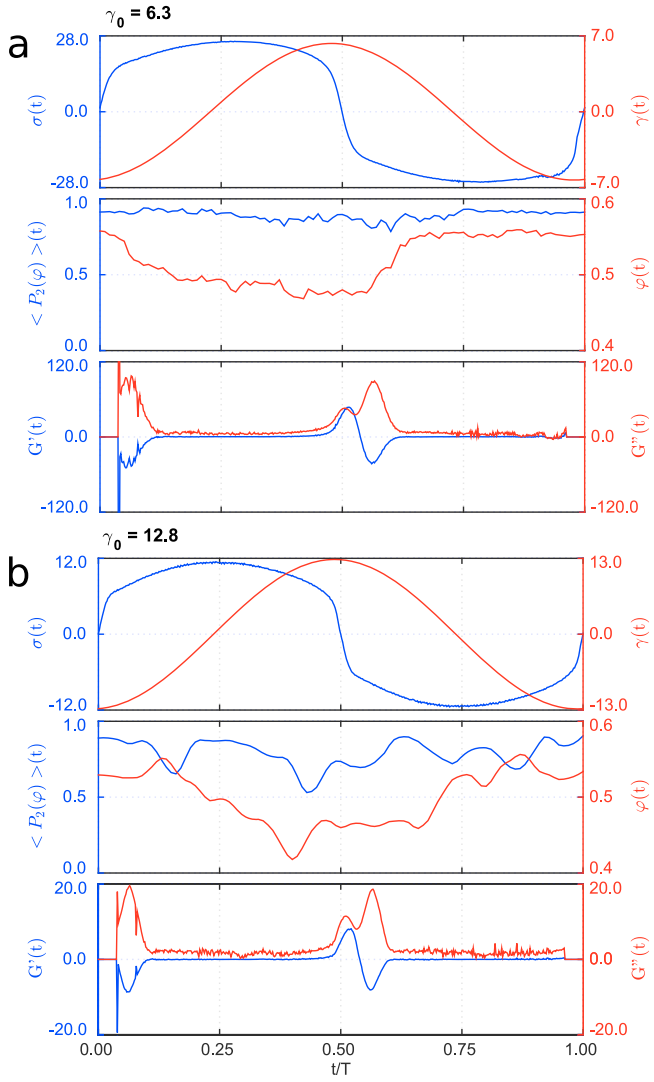

FIG. 10. Responses of strain controlled experiments at approximately same strain amplitude as in the stress controlled $\mathbf{v} - \nabla\mathbf{v}$ plane, left side of Fig. 6.

V. DISCUSSION

We learned that the dynamic yielding of the strong anchoring system of nematic platelets is a multi-step process with anomalous structural and mechanical responses. The *first yielding transition* of the structure, indicated by the start of the red sequence in Fig. 11, is from a completely quiescent structure at small stress amplitude to a jittering motion of the director in the $\mathbf{v} - \nabla\mathbf{v}$ plane at intermediate stress amplitude. The structural signature of this behavior in the $\mathbf{v} - \nabla \times \mathbf{v}$ plane is a first harmonic structural response. This structural bifurcation is accompanied by a change in the mechanical response, such that the amplitude of the strain response, $\Delta\gamma$, becomes more symmetrical, while the symmetry in time changes from a spinning sidle to a spinning hop. The other mechanical signature of the first yielding transition is the crossing of $J'(t)$ with $J''(t)$, confirmed by the crossing in J' with J'' calculated in the conventional manner, see Fig. 2(b). The *second yielding transition*, indicated by the start of green sequence in Fig. 11, increasing the stress amplitude to values well above the static yield stress, is characterized by a bifurcation in the motion of the director. It oscillates between a wall-anchored state and a flowing state in the $\mathbf{v} - \nabla\mathbf{v}$ plane, while a second harmonic response is observed in the $\mathbf{v} - \nabla \times \mathbf{v}$ plane. Mechanically, the offset of $\Delta\gamma$ approaches 0, i.e., the response becomes symmetrical, and around flow reversal there is a time window where there is no elasticity as $J'(t) \approx 0$. A *third yield transition* is observed, indicated by the start of the blue sequence in Fig. 11, which we did not fully capture indicated by the start of the blue dashed sequence in Fig. 11, when giving sufficient time to the system to respond. In this case, the nematic director will be able to undergo full oscillations around the wall-anchored state, in contrast to the strain response which becomes completely offset. Thus, for stress controlled experiments, frequency and stress amplitude are equally important parameters for the system to yield, more so than for LAOStrain experiments, where the system is forced to yield.

It is conceivable that the rich yielding behavior of our nematic platelet system is connected with the strong wall anchoring of such a system.[43] It can be theoretically shown that indeed, wall anchoring of a nematic system can cause rich dynamic behavior when the nematic is sheared, depending on, for example, the angle of alignment at the wall.[44,45] Indeed, multiple-yielding processes have recently been observed in magneto-rheological measurements on platelet particles, where the magnetic field basically plays the role of enhancing the wall anchoring.[46] In addition, it has been shown that the yielding behavior of concentrated platelet suspensions is related to the structural changes of the aligned domains, as a result of the competition between network build-up due to globally low entropy or the breakup of the network under flow.[47,48] Less related but equally interesting is the "house of cards" effect of platelets that undergoes a rheological bifurcation at a critical stress where the viscosity jumps to infinity, followed by a rapid drop as the system starts to flow.[2] All of these studies are mainly rheological and lack structural support. SAXS and SANS proved to be very useful tools to obtain structural information of sheared nematics, as was shown in the case of colloidal platelets.[1,49,50] In order to capture, however, a complete picture of the physics behind complex events as this above described multiple yielding, it is crucial to obtain structural information in all relevant scattering planes, including the $\mathbf{v} - \nabla\mathbf{v}$ plane, while controlling the stress on the sheared sample.

Thus, the work presented here represents an important development in the field. Most *in situ* experiments either have full rheological control but are limited in the accessible scattering geometries,[51] while the *in situ* experiments that do access the relevant geometries do not have rheological control and rely on the use of shear cells.[52–55] With our experiments we not only show that it is of crucial importance to probe structure in all relevant scattering planes but also that is important to be able to control the stress while doing so.

Another novelty of this work concerns the analysis of the mechanical response. We introduce a new analysis method of the rheological response in order to facilitate the comparison of mechanical and structural responses throughout the full period of the oscillating field. The nonlinear response can be revealed by using the analysis method for mechanical characterization proposed by Rogers,[6] calculating the instantaneous compliances $J'(t)$ and $J''(t)$, that includes contributions

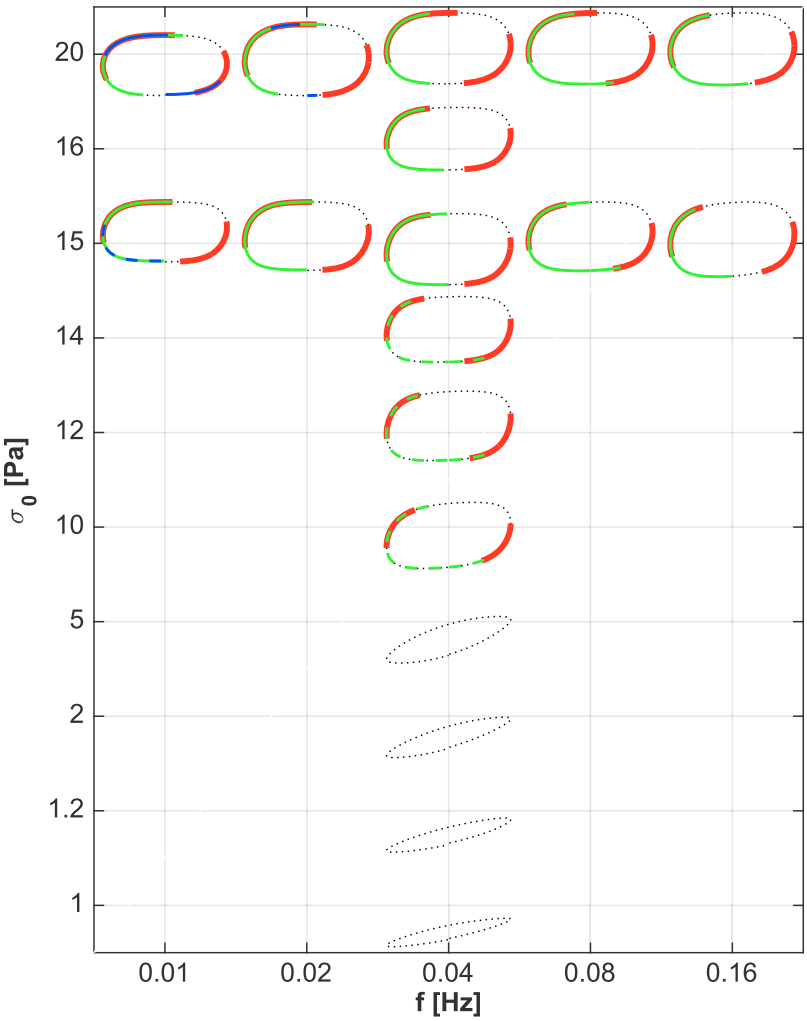

FIG. 11. Pipkin diagram for all LAOStress responses. The start of the three colored segments indicates the yielding transitions, while the length indicates the time window over which the features ($J'(t) < J''(t)$ in red, nematic director oscillating between a wall-anchored state and a flowing state in green, and $\Delta\varphi$ symmetry in blue) hold.

from all harmonics. Furthermore, this method allows for all responses to be considered, independent of their symmetry in time, unlike the Fourier based methods that require certain symmetries. Indeed, we indicate the richness in symmetries depending on the degree of yielding. This novel time-dependent approach enables us to identify intervals where the systems become completely elastic or plastic and compare those states with the structure at the same time.

Further studies are necessary to fully capture the impact of wall anchoring onto the yielding of the system, especially focusing on the relation between the flow profile and local structure, relying on techniques like X-ray photon correlation spectroscopy.[56,57]

VI. CONCLUSION

In conclusion, we revealed the dynamic yielding of a nematic dispersion of gibbsite particles, which is a strong anchoring system, to large amplitude stress oscillations. We monitored both the mechanical and structural responses *in situ*, combining a stress controlled rheometer with a vertical beam SAXS. We have access to the full 3D rotational motion of the nematic director via the use of multiple geometries and a vertical beam. We identified multiple yielding transitions that depend both on the amplitude of the oscillation and the frequency.

SUPPLEMENTARY MATERIAL

See supplementary material for visualization of the structure and rheology as the nematic domains split up after flow reversal at applied stress amplitudes above the yield stress.

ACKNOWLEDGMENTS

O.K. acknowledges the International Helmholtz Research School of Biophysics and Soft Matter for financial support. Wim Bras and Giuseppe Portale are thanked for the experimental support at ESRF.

NOMENCLATURE

$\mathbf{n}$	= Nematic director
φ_{max} (rad)	= Nematic director's azimuthal angle
θ_{max} (rad)	= Nematic director's polar angle
ψ_{max} (rad)	= Scattering projection on the $\mathbf{v} - \boldsymbol{\nabla} \times \mathbf{v}$ plane
$\varphi(t)$, $\psi(t)$ (rad)	= Instantaneous angles
$f(\varphi, \theta)$	= Orientational distribution function
$I(\psi\|_{q_{max}})$, $I(\varphi\|_{q_{max}})$ (a.u.)	= Scattering intensity at qmax vs. angle

$\langle P_2(\psi)\rangle$	= Average orientational order parameter along ψ
$\langle P_2(\varphi)\rangle$	= Average orientational order parameter along φ
$\Delta\varphi_{peak}$, $\Delta\varphi_{plateau}$ (rad)	= Amplitude in φ peak-peak and plateau-plateau
φ_{offset}, $\varphi_{offset-peak}$ (rad)	= Vertical offset in $\varphi(t)$ plateau-plateau or peak-to-peak
$\Delta I_{plateau}$, ΔI_{peak} (a.u.)	= Scattering amplitude at $\varphi_{plateau}$ or φ_{peak}
η (Pa s)	= Viscosity
J' (Pa^{-1})	= Storage compliance
J'' (Pa^{-1})	= Loss compliance
σ_0 (Pa)	= Applied stress amplitude
$\sigma(t)$ (Pa)	= Instantaneous shear stress
$\gamma(t)$	= Instantaneous shear strain
$\Delta\gamma$	= Shear strain amplitude
γ_{offset}	= Vertical offset in $\gamma(t)$
$J'(t)$(Pa^{-1})	= Instantaneous storage compliance
$J''(t)$ (Pa^{-1})	= Instantaneous loss compliance
$\Delta J'$ (Pa^{-1})	= Storage compliance amplitude
$G'(t)$ (Pa)	= Instantaneous storage modulus
$G''(t)$ (Pa)	= Instantaneous loss modulus

[1] L. J. Michot, C. Baravian, I. Bihannic, S. Maddi, C. Moyne, J. F. L. Duval, P. Levitz, and P. Davidson, "SolGel and isotropic/nematic transitions in aqueous suspensions of natural nontronite clay. Influence of particle anisotropy. 2. Gel structure and mechanical properties," Langmuir **25**, 127–139 (2009).

[2] P. Coussot, Q. D. Nguyen, H. T. Huynh, and D. Bonn, "Avalanche behavior in yield stress fluids," Phys. Rev. Lett. **88**, 175501 (2002).

[3] A. J. W. ten Brinke, L. Bailey, H. N. W. Lekkerkerker, and G. C. Maitland, "Rheology modification in mixed shape colloidal dispersions. I. Pure components," Soft Matter **3**, 1145 (2007).

[4] F. M. van der Kooij, D. van der Beek, and H. N. W. Lekkerkerker, "Isotropic-nematic phase separation in suspensions of polydisperse colloidal platelets," J. Phys. Chem. B **105**, 1696–1700 (2001).

[5] M. P. Lettinga, P. Holmqvist, P. Ballesta, S. Rogers, D. Kleshchanok, and B. Struth, "Nonlinear behavior of nematic platelet dispersions in shear flow," Phys. Rev. Lett. **109**, 246001 (2012).

[6] S. A. Rogers, "A sequence of physical processes determined and quantified in Laos: An instantaneous local 2D/3D approach," J. Rheol. **56**, 1129 (2012).

[7] D. J. Plazek, "What's wrong with the moduli Charley Brown? or Get the H out and go to L," J. Rheol. **36**, 1671 (1992).

[8] C. J. Dimitriou, R. H. Ewoldt, and G. H. McKinley, "Describing and prescribing the constitutive response of yield stress fluids using large amplitude oscillatory shear stress (LAOStress)," J. Rheol. **57**, 27 (2013).

[9] R. H. Ewoldt, "Defining nonlinear rheological material functions for oscillatory shear," J. Rheol. **57**, 177 (2013).

[10] K. Hyun, M. Wilhelm, C. O. Klein, K. S. Cho, J. G. Nam, K. H. Ahn, S. J. Lee, R. H. Ewoldt, and G. H. McKinley, "A review of nonlinear oscillatory shear tests: Analysis and application of large amplitude oscillatory shear (LAOS)," Prog. Polym. Sci. **36**, 1697–1753 (2011).

[11] S. A. Rogers and M. P. Lettinga, "A sequence of physical processes determined and quantified in large-amplitude oscillatory shear (LAOS): Application to theoretical nonlinear models," J. Rheol. **56**, 1 (2012).

[12] J. Läuger and H. Stettin, "Differences between stress and strain control in the non-linear behavior of complex fluids," Rheol. Acta **49**, 909–930 (2010).

[13] J. E. Bae, M. Lee, K. S. Cho, K. H. Seo, and D. G. Kang, "Comparison of stress-controlled and strain-controlled rheometers for large amplitude oscillatory shear," Rheol. Acta **52**, 841–857 (2013).

[14] P. R. de Souza Mendes, R. L. Thompson, A.A. Alicke, and R. T. Leite, "The quasilinear large-amplitude viscoelastic regime and its significance in the rheological characterization of soft matter," J. Rheol. **58**, 537–561 (2014).

[15] D. Merger and M. Wilhelm, "Intrinsic nonlinearity from LAOS-trainexperiments on various strain- and stress-controlled rheometers: A quantitative comparison," Rheol. Acta **53**, 621–634 (2014).

[16] R. H. Ewoldt, M. T. Johnston, and L. M. Caretta, "Experimental challenges of shear rheology: How to avoid bad data," in *Complex Fluids in Biological Systems* (Springer New York, 2015) Chap. 9, pp. 207–241.

[17] P. Coussot, Q. D. Nguyen, H. T. Huynh, and D. Bonn, "Viscosity bifurcation in thixotropic, yielding fluids," J. Rheol. **46**, 573 (2002).

[18] F. Da Cruz, F. Chevoir, D. Bonn, and P. Coussot, "Viscosity bifurcation in granular materials, foams, and emulsions," Phys. Rev. E **66**, 051305 (2002).

[19] J. Sprakel, S. B. Lindström, T. E. Kodger, and D. A. Weitz, "Stress enhancement in the delayed yielding of colloidal gels," Phys. Rev. Lett. **106**, 1–4 (2011).

[20] B. Struth, K. Hyun, E. Kats, T. Meins, M. Walther, M. Wilhelm, and G. Grubel, "Observation of new states of liquid crystal 8CB under nonlinear shear conditions as observed via a novel and unique rheology/small-angle x-ray scattering combination," Langmuir **27**, 2880–2887 (2011).

[21] W. Bras, I. Dolbnya, D. Detollenaere, R. van Tol, M. Malfois, G. Greaves, A. Ryan, and E. Heeley, "Recent experiments on a small-angle/wide-angle x-ray scattering beam line at the ESRF," J. Appl. Crystallogr. **36**, 791–794 (2003).

[22] G. Portale, D. Cavallo, G. C. Alfonso, D. Hermida-Merino, M. van Drongelen, L. Balzano, G. W. M. Peters, J. G. P. Goossens, and W. Bras, "Polymer crystallization studies under processing-relevant conditions at the SAXS/WAXS DUBBLE beamline at the ESRF," J. Appl. Crystallogr. **46**, 1681–1689 (2013).

[23] D. Pennicard, S. Lange, S. Smoljanin, H. Hirsemann, H. Graafsma, M. Epple, M. Zuvic, M.-O. Lampert, T. Fritzsch, and M. Rothermund, "The LAMBDA photon-counting pixel detector," J. Phys.: Conf. Ser. **425**, 062010 (2013).

[24] D. Pennicard, S. Smoljanin, B. Struth, H. Hirsemann, A. Fauler, M. Fiederle, O. Tolbanov, A. Zarubin, A. Tyazhev, G. Shelkov, and H. Graafsma, "The LAMBDA photon-counting pixel detector and high-Z sensor development," J. Instrum. **9**, C12026 (2014).

[25] M. C. D. Mourad, D. V. Byelov, A. V. Petukhov, and H. N. W. Lekkerkerker, "Structure of the repulsive gel/glass in suspensions of charged colloidal platelets," J. Phys.: Condens. Matter **20**, 494201 (2008).

[26] D. Kleshchanok, J.-M. Meijer, A. V. Petukhov, G. Portale, and H. N. W. Lekkerkerker, "Attractive glass formation in aqueous mixtures of colloidal gibbsite platelets and silica spheres," Soft Matter **7**, 2832 (2011).

[27] S. A. Rogers and D. Vlassopoulos, "Frieze group analysis of asymmetric response to large-amplitude oscillatory shear," J. Rheol. **54**, 859 (2010).

[28] P. Davidson, D. Petermann, and A. M. Levelut, "The measurement of the nematic order parameter by x-ray scattering reconsidered," J. Phys. II **5**, 113–131 (1995).

[29] W. Philippoff, "Vibrational measurements with large amplitudes," J. Rheol. **10**, 317 (1966).

[30] J. Harris and K. Bogie, "The experimental analysis of non-linear waves in mechanical systems," Rheol. Acta **6**, 3–5 (1967).

[31] J. S. Dodge, "Oscillatory shear of nonlinear fluids I. Preliminary investigation," J. Rheol. **15**, 589 (1971).

[32] W. C. MacSporran and R. P. Spiers, "The dynamic performance of the Weissenberg rheogoniometer. II. Large amplitude oscillatory shearing—Fundamental response," Rheol. Acta **21**, 193–200 (1982).

[33] J. M. Dealy and K. F. Wissbrun, *Melt Rheology and Its Role in Plastics Processing* (Springer, Netherlands, Dordrecht, 1990).

[34] K. S. Cho, K. Hyun, K. H. Ahn, and S. J. Lee, "A geometrical interpretation of large amplitude oscillatory shear response," J. Rheol. **49**, 747 (2005).

[35] R. H. Ewoldt, A. E. Hosoi, and G. H. McKinley, "New measures for characterizing nonlinear viscoelasticity in large amplitude oscillatory shear," J. Rheol. **52**, 1427 (2008); e-print arxiv:0710.5509.

[36] S. A. Rogers, B. M. Erwin, D. Vlassopoulos, and M. Cloitre, "A sequence of physical processes determined and quantified in LAOS: Application to a yield stress fluid," J. Rheol. **55**, 435 (2011).

[37] A. S. Poulos, J. Stellbrink, and G. Petekidis, "Flow of concentrated solutions of starlike micelles under large-amplitude oscillatory shear," Rheol. Acta **52**, 785–800 (2013).

[38] K. van der Vaart, Y. Rahmani, R. Zargar, Z. Hu, D. Bonn, and P. Schall, "Rheology of concentrated soft and hard-sphere suspensions," J. Rheol. **57**, 1195–1209 (2013).

[39] J. Min Kim, A. P. R. Eberle, A. Kate Gurnon, L. Porcar, and N. J. Wagner, "The microstructure and rheology of a model, thixotropic nanoparticle gel under steady shear and large amplitude oscillatory shear (LAOS)," J. Rheol. **58**, 1301–1328 (2014).

[40]J. H. Conway, "The orbifold notation for surface groups," in *Groups, Combinatorics and Geometry*, Proceedings of the L.M.S. Durham Symposium, Durham, UK, 5–15, July 1990, L.M.S. Lecture Notes Series 165, edited by M. W. Liebeck and J. Saxl (Cambridge University Press, Cambridge, Durham, UK, 1992), pp. 438–447.
[41]J. H. Conway and D. H. Huson, "The orbifold notation for two-dimensional groups," Struct. Chem. **13**, 247–257 (2002).
[42]F. M. Leslie, "Some constitutive equations for liquid crystals," Arch. Ration. Mech. Anal. **28**, 265–283 (1967).
[43]D. Van Der Beek, P. Davidson, H. H. Wensink, G. J. Vroege, and H. N. W. Lekkerkerker, "Influence of a magnetic field on the nematic phase of hard colloidal platelets," Phys. Rev. E **77**, 031708 (2008).
[44]S. Heidenreich, S. Hess, and S. H. L. Klapp, "Shear-induced dynamic polarization and mesoscopic structure in suspensions of polar nanorods," Phys. Rev. Lett. **102**, 028301 (2009).
[45]E. P. Choate and M. G. Forest, "Dependence of the dynamic moduli of heterogeneous nematic polymers on planar anchoring relative to flow direction," Rheol. Acta **50**, 767–778 (2011).
[46]I. Arief and P. Mukhopadhyay, "Two-step yielding in novel CoNi nanoplatelet-based magnetic fluids under oscillatory rheology," Mater. Lett. **167**, 192–196 (2016).
[47]M. Moan, T. Aubry, and F. Bossard, "Nonlinear behavior of very concentrated suspensions of plate-like kaolin particles in shear flow," J. Rheol. **47**, 1493 (2003).
[48]F. Bossard, M. Moan, and T. Aubry, "Linear and nonlinear viscoelastic behavior of very concentrated plate-like kaolin suspensions," J. Rheol. **51**, 1253 (2007).
[49]A. B. D. Brown and A. R. Rennie, "Monodisperse colloidal plates under shear," Phys. Rev. E **62**, 851–862 (2000).
[50]A. B. D. Brown and A. R. Rennie, "Images of shear-induced phase separation in a dispersion of hard nanoscale discs," Chem. Eng. Sci. **56**, 2999–3004 (2001).
[51]V. Herle, J. Kohlbrecher, B. Pfister, P. Fischer, and E. J. Windhab, "Alternating vorticity bands in a solution of wormlike micelles," Phys. Rev. Lett. **99**, 1–4 (2007).
[52]F. E. Caputo and W. R. Burghardt, "Real-time 1-2 plane SAXS measurements of molecular orientation in sheared liquid crystalline polymers," Macromolecules **34**, 6684–6694 (2001).
[53]M. W. Liberatore, F. Nettesheim, N. J. Wagner, and L. Porcar, "Spatially resolved small-angle neutron scattering in the 1-2 plane: A study of shear-induced phase-separating wormlike micelles," Phys. Rev. E **73**, 020504(R) (2006).
[54]M. W. Liberatore, F. Nettesheim, P. A. Vasquez, M. E. Helgeson, N. J. Wagner, E. W. Kaler, L. P. Cook, L. Porcar, and Y. T. Hu, "Microstructure and shear rheology of entangled wormlike micelles in solution," J. Rheol. **53**, 441–458 (2009).
[55]M. E. Helgeson, M. D. Reichert, Y. T. Hu, and N. J. Wagner, "Relating shear banding, structure, and phase behavior in wormlike micellar solutions," Soft Matter **5**, 3858 (2009).
[56]M. C. Rogers, K. Chen, L. Andrzejewski, S. Narayanan, S. Ramakrishnan, R. L. Leheny, and J. L. Harden, "Echoes in x-ray speckles track nanometer-scale plastic events in colloidal gels under shear," Phys. Rev. E **90**, 062310 (2014).
[57]F. Westermeier, D. Pennicard, H. Hirsemann, U. H. Wagner, C. Rau, H. Graafsma, P. Schall, M. Paul Lettinga, and B. Struth, "Connecting structure, dynamics and viscosity in sheared soft colloidal liquids: A medley of anisotropic fluctuations," Soft Matter **12**, 171–180 (2016).